 doi:10.20944/preprints202103.0057.v1

Review

Lightinduced effects in amorphous chalcogenide glasses: Femtoseconds to seconds

Pritam Khan [1,*] and K. V. Adarsh [2,*]

[1] Department of Physics and Bernal Institute, University of Limerick, Limerick V94T9PX, Ireland; Pritam.Khan@ul.ie
[2] Department of Physics, Indian Institute of Science Education and Research Bhopal 462066. India; adarsh@iiserb.ac.in
* Correspondence: Pritam.Khan@ul.ie and adarsh@iiserb.ac.in

Abstract: Amorphous chalcogenide (ChGs) glasses are intrinsically metastable, highly photosensitive, and therefore exhibit numerous lightinduced effects upon bandgap and sub-bandgap illumination. Depending on the pulse duration of the excitation laser, ChGs exhibit a series of lightinduced effects spanning over femtosecond to seconds time domain. For continuous wave illumination, the effects are dominantly metastable in terms of photodarkening (PD) and photobleaching (PB) that takes place via homopolar to heteropolar bond conversion. On the other hand, under nanosecond and ultrafast pulsed illumination, ChGs exhibit transient absorption (TA) that is instigated from the transient bonding rearrangements through self-trapped exciton recombination. In the first part of the review, we pay special attention to continuous wave lightinduced PD and PB, while in the second part we will focus on the TA and controlling such effects via internal and external parameters e.g., chemical composition, temperature, sample history etc.

Keywords: chalcogenide glasses; pump-probe; photodarkening; photobleaching; transient absorption, network rigidity

1. Introduction

ChGs consists of covalently bonded chalcogen elements which belong to the group VI of the periodic table-Sulphur (S), Selenium (Se), and Tellurium (Te) and formed in conjugation with the elements of group V (Sb, As) or group IV (Ge, Si) [1]. The bandgap of the ChG lie within the range of 1–3 eV [2]. ChG possess a remarkable property of transparency in the wide Infrared (IR) region which makes them a promising candidate for infrared cameras [3], planar waveguides for integrated optics [4] and infrared sensors [5]. Additionally, these glasses have high chemical resistance to extremely corrosive media, and they can tune their physical and chemical properties over a wide range by changing the composition [6,7]. Among the several families of ChG, the most widely studied systems are the binary As-S (Se) and Ge-S (Se), the ternary Ge-As-S (Se) and Ge-Sb-Te (Se, S).

ChG are distinguished from other materials by their unique photosensitivity to bandgap or sub-bandgap illumination that is depicted by numerous photo-induced effects related its structure and properties [1,8]. Photoinduced processes are typically linked with the changes in optical parameters, mainly the bandgap energy and variation of the refractive index. Photoinduced changes in amorphous ChG are associated with the generation of electron-hole (e-h) pairs [9,10]. The absorption of a photon may result in the forming, separating, or recombining of an electron-hole pair. Separation of e-h pair leads to changes in the electrical response of the material that may give rise to photoconductivity [11]. On the other hand, radiative e-h recombination leads to photoluminescence, whereas non-radiative recombination of e-h pair results in photostructural and optical changes in the material [12].

Preprints (www.preprints.org) | NOT PEER-REVIEWED | Posted: 2 March 2021 doi:10.20944/preprints202103.0057.v1

Photoinduced effects in ChG are generally classified in terms of the reversibility/irreversibility. The reversibility is defined by its ability to recover to the initial state, i.e., before irradiation. Reversible effects are of two types: metastable and transient. Metastable effects can be recovered by heating the material near the glass transition temperature (T_g), whereas transient effects persist only during illumination [13]. In contrast, irreversible effects are mostly permanent changes that can only be reversed by heating it above T_g, even close to the melting point of the sample.

Metastable and transient photoinduced effects can also be distinguished by varying the pulse width of the excitation laser. Depending on the duration of the laser pulses photoinduced effects vary significantly. It was shown by numerous previous studies that the photodarkening (PD) and photobleaching (PB) are the two light-induced effects unique to ChG when illuminated with continuous wave bandgap or sub-bandgap light [8,13,14]. On the other hand, for nanosecond and ultrafast pulsed laser illumination transient absorption (TA) is most commonly observed [15,16]. In this review, we will discuss the time evolution of photoinduced effects in ChGs in two parts. In the first part, we will discuss CW laser induced PD and PB that takes place between seconds to hours, while in the second part we focus on TA and its evolution in picosecond to microsecond time scale.

2. Continuous wave (CW) lightinduced effects in ChGs

PD and PB are characterized by the lightinduced shift in the absorption edge towards longer and shorter wavelengths. PD is defined by a reduction of optical bandgap, i.e., absorption edge of the material red shifts, to longer wavelengths or lower photon energies and the material becomes darker with decrease in transmission [13,14]. The phenomenon of PD was first reported by Berkes *et al*. [17] on a 1 μm film of As_2Se_3 that was exposed to focused microscope light. PD is mostly observed in the arsenic (As) based ChG and is believed to originate from lightinduced reduction of homopolar bonds to energetically favorable heteropolar bonds [18,19]:

$$As_{(x-y)}C_z + yAs + h\nu \leftrightarrow As_xC_z \tag{1.12}$$

Here 'C' represents the chalcogen element. Importantly, PD consists of a transient and metastable part [14,18,20]. When illumination is switched off after the complete saturation of PD, there is an appreciable transient decay, but some switched bonds remain frozen in a metastable state that can only be reversed by annealing the sample near T_g [13].

In stark contrast to PD, PB is characterized by a blue shift (to shorter wavelength) of the optical absorption edge, i.e., the optical bandgap of the material increases, and sample becomes transparent, i.e., transmission increases [8,21]. Unlike PD, PB cannot be reversed by heat treatment. PB is most commonly observed in germanium (Ge) based ChG which can be understood in terms of two parallel mechanisms. First is intrinsic structural changes described by the following equation [18,22]:

$$Ge - Ge + Se - Se + h\nu \leftrightarrow 2Ge - Se \tag{1.13}$$

The second includes the photo-oxidation of Ge atoms by the creation of Ge-O bonds at the expense of Ge-Ge bonds that are broken by illumination [22-24]. PB is very sensitive to material composition and deposition technique. Importantly, the refractive index of the material changes upon PD/PB which might be useful for fabricating optical devices.

2.1. Photodarkening in As-based ChGs

As_2S_3 and As_2Se_3 are most commonly known As-based ChGs, which are studied extensively for the lightinduced effects [13,25,26]. In-situ transmission measurements, in other words CW pump-probe measurements are often used to demonstrate the lightinduced effects in ChGs. It can be seen from Fig. 1(a) that transmission spectra of As_2Se_3 ChG thin films near the optical absorption edge gradually redshifts upon 660 nm CW laser illumination to demonstrate PD [26]. This leads to associated decrease in transmission as shown in Fig. 1(b) at three different fixed probe wavelengths. Clearly, when the laser is switched on, for all the wavelengths, transmission decreases continuously before reaching a plateau. Similar PD is also observed in As_2S_3 as demonstrated by the work of Ganjoo

Preprints (www.preprints.org) | NOT PEER-REVIEWED | Posted: 2 March 2021 doi:10.20944/preprints202103.0057.v1

and Jain [13]. When illuminated with 488 nm CW laser, optical transmission spectra of As_2S_3 redshifts (Fig. 1(c)), characteristic of PD. The bottom left panel of Fig. 1(c) showed the zoomed region focusing the optical absorption edge near the bandgap. Likewise, following laser illumination, transmission decreases at all probe wavelengths as shown in the bottom right panel of Fig. 1(c). It is important to note that, lightinduced effect consists of two part: transient and metastable. The transient component exists only during illumination while the existing permanent changes after illumination is referred as metastable. We will discuss both of these in the following section.

Figure 1. (a) Transmission spectra of a-As_2Se_3 films at laser intensity 10 mW/cm^2. The red arrow indicates the shift in transmission spectra. (b) Variation in transmission as a function of time at wavelengths 580, 600, and 610 nm for the intensity 10 mW/cm^2. All the figures were reprinted (adapted) with permission from [26] Copyright 2009, American Institute of Physics. (c) Transmission spectra for a-As_2S_3 films before (— — —-), during (at t=1 sec (- - - - - -), 60 sec (• • • • • • • •), 3600 sec (– • – • – •) and after illumination (- - - - - -). The spectrum before switching off the illumination (– • – • –) is recovered when the exciting laser is switched on again (– - - – - - –). Expanded part of the spectra between 450 and 500 nm and variation of transmission as a function of time at the indicated wavelengths. (d) Variation of absorption coefficient with time at indicated wavelengths. The laser ON and OFF states are indicated in the figure. Inset shows the decay and rise of the transient part of the changes on linear time scale when the exciting laser is switched off and on repeatedly. All the figures were reprinted (adapted) with permission from [13] Copyright 2006, American Physical Society. (e) Time variation in the changes in optical band gap (E_g) for different laser intensity. The solid black circle shows the optical band gap before the exciting laser is switched on. All the figures were reprinted (adapted) with permission from [26] Copyright 2009, American Institute of Physics. (f) Time variation of the changes in refractive index (n) at 633 nm during and after illumination. The solid line is theoretical fit. The solid black circle shows the refractive index before the exciting laser is switched on. Inset shows the decay and the rise of the transient part of the changes on linear time scale when the exciting laser is switched off and on. All the figures were reprinted (adapted) with permission from [13] Copyright 2006, American Physical Society. (g) Change in refractive index as a function of wavelength. All the figures were reprinted (adapted) with permission from [27] Copyright 2002, The Optical Society.

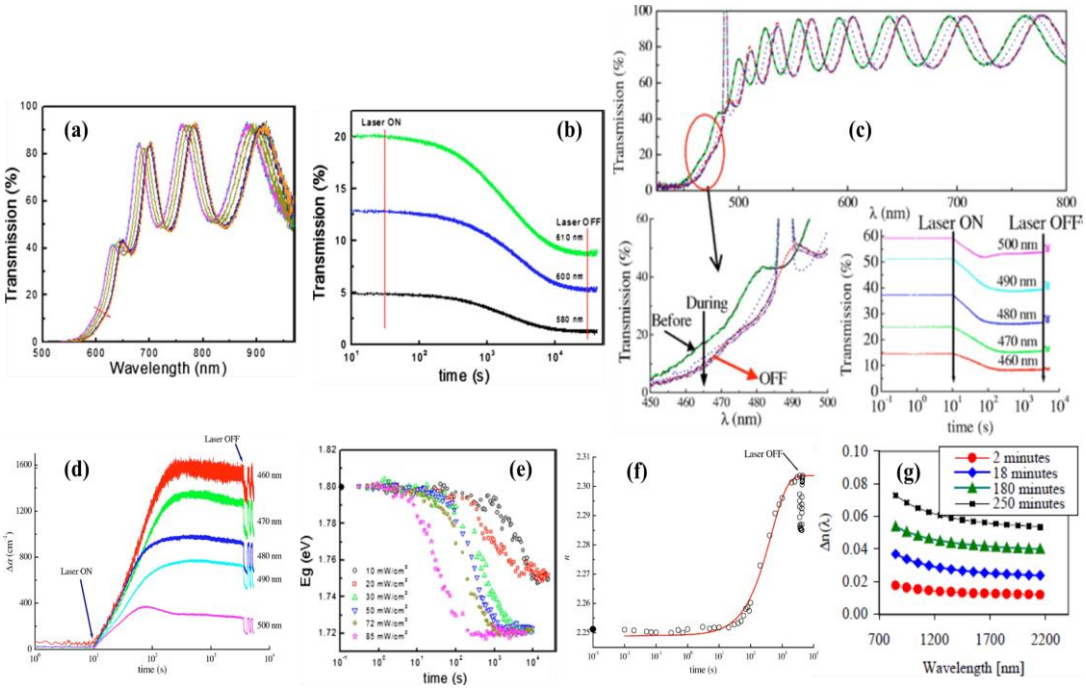

Similar to transmission, PD leads to a change in absorption coefficient $\Delta\alpha$ for all probe wavelengths. Since $\Delta\alpha=(-1/d)\ln(T/T_0)$, (d=thickness of the film) decrease in transmission is reflected by the increase in $\Delta\alpha$ upon PD as shown in Fig. 1(d). The transient part of the changes is understood from the several on-off cycles of laser illumination which

Preprints (www.preprints.org) | NOT PEER-REVIEWED | Posted: 2 March 2021 doi:10.20944/preprints202103.0057.v1

are further zoomed in the inset. When laser is switched on, $\Delta\alpha$ increases monotonically and reaches a plateau. When the laser is switched off, $\Delta\alpha$ decreases and saturates quickly but never reaches the value before the illumination. This decrease part of $\Delta\alpha$ is termed as transient while the saturated portion remained after illumination is defined as metastable. When the laser is switched on subsequently, $\Delta\alpha$ increases again and transient part reappears reaching the same value as the saturated value in the first illumination. Noteworthy to mention, repeated on and off cycles only induced the transient part.

Since the absorption coefficient $\Delta\alpha$ changes significantly near the optical absorption edge, bandgap of the material also changes following PD. Fig. 1(e) shows the time evolution of optical bandgap (E_g) in As_2S_3 [26]. Clearly, E_g decreases slowly for the initial period which is followed by s steep decreases before reaching the plateau. The change in bandgap is higher as well as faster for higher laser intensity (pink curve) and less and slower for lower intensities. Quantitatively, Sati *et al*. [26] demonstrated that change in bandgap ΔE_g is 0.05 eV at a laser intensity of 10 mW/cm^2 whereas it increases to 0.08 eV when illuminated with intensity of 85 mW/cm^2. In addition, characteristic decay time of PD also changes dramatically, e.g., kinetics of PD becomes faster from 3600 s to 50 s when intensity increases from 10 to 85 W/cm^2.

Refractive index (n) is another important optical constant that changes significantly upon PD as shown by the Fig. 1(f). For practical application of ChGs in integrated optics it is important to have the detailed understanding on the dynamic changes of n. Ganjoo and Jain [13] estimated the change the n from the fringes of the transmission spectra in Fig. 1(c) by employing Swanepoel method [28]. Following laser illumination, n initially increases slowly and then increases rapidly before reaching the plateau. Notably, n also comprises of transient and metastable component like other optical parameters. Popta *et al*. [27] showed the wavelength dependence of the n in As_2Se_3 thin films by plotting it over a broad wavelength regime in NIR as shown in Fig. 1(g). The curve demonstrates the magnitude of the change in the real part of the refractive index at different exposure times, which is measured by subtracting from the as-prepared value before laser illumination. Since the bandgap of As_2Se_3 is 1.76 eV (704 nm), the refractive index expected increases near the band edge toward 700 nm following Kramers-Kronig relationship [29].

2.2. Photobleaching in Ge-based ChGs

Photobleaching (PB) in Ge based ChGs was first observed by Lyubin in $GeSe_2$ thin films 488 nm CW laser [21]. Similar PB was later observed by in $GeSe_2$ by Barik et al. using 532 nm CW laser [30]. The more detailed study on PB was performed by Yan and coworkers in $GeSe_2$ as well as in Ge rich Ge_2Se_3 [22]. Fig. 2 (a) and (b) shows the optical transmission spectra of $GeSe_2$ and Ge_2Se_3 thin films in as-prepared and when illuminated with 488 nm and 660 nm laser, respectively. Clearly, for the initial period of illumination, the spectra remains indistinguishable however with prolonged illumination, transmission spectra blueshift, a signature of PB. To get detailed understanding on the kinetics of PB, they recorded the time evolution of the transmission at fixed probe wavelengths for both $GeSe_2$ and Ge_2Se_3 as shown in Fig. 2(c) and (d) respectively. Clearly, for both the sample, after a initial dip transmission increases gradually and final saturated transmission is much higher that initial transmission in line with PB. When the laser is turned off, transmission increases further and the transient component saturates very quickly. Unlike PD, PB is belived to be originated not only from structural changes (Ge-Ge to Ge-Se) but also from the surface photooxidation of Ge atoms, i.e. formation of Ge-O bonds. In this regard, Fig. 2(e) demonstrates the IR difference spectra before and after illumination for the samples. Since Ge_2Se_3 is rich in Ge-Ge bonds, photooxidation in perdominant which is evinced by the strong GeO_2 structural unit at 870 cm^{-1}. On the other hand, in $GeSe_2$ because of lesser Ge content, oxidation takes place by forming chains of Se_{3-x}-O_x-Ge-O-Ge-O_x-Se_{3-x} clusters at 820 cm^{-1} [24,31]. Much later we quantitatively demonstarted the relative contrbution of structrual changes and photooxidation to PB in $Ge_{25}As_{10}Se_{65}$ thin films [32]. We recorded the in-situ transmission changes in air and in vacuum, where the oxygen concentration is negligible and relative single wavelength transmission kinetics is shown

Preprints (www.preprints.org) | NOT PEER-REVIEWED | Posted: 2 March 2021 doi:10.20944/preprints202103.0057.v1

in Fig. 2(f). We found that magnitude of PB in air (ΔPB=0.21) is much larger compared to the magnitude in the vacuum (ΔPB=0.13), i.e. 62% of total changes in PB is associated with structural changes while photooxidation plays the minor role in PB. Additioanlly, since the photooxidation is a slower process, it makes the kinetics of PB in air (τ_{air} = 1896 s) about ten times slower than in vacuum (τ_{air} = 210 s).

Figure 2. Changes in the full transmission spectra for (a) $GeSe_2$ and (b) Ge_2Se_3 films upon exposure in air. Time variation of transmission for as-deposited (c) $GeSe_2$ and (d) Ge_2Se_3 films illuminated in air. (e) IR difference absorption spectra (after-before illumination) for $GeSe_2$ (solid line) and Ge_2Se_3 (dashed line) films. All the figures were reprinted (adapted) with permission from [22] Copyright 2011, American Chemical Society. (f) The comparative lightinduced effects in a-$Ge_{25}As_{10}Se_{65}$ thin films when illuminated in the vacuum and in air. All the figures were reprinted (adapted) with

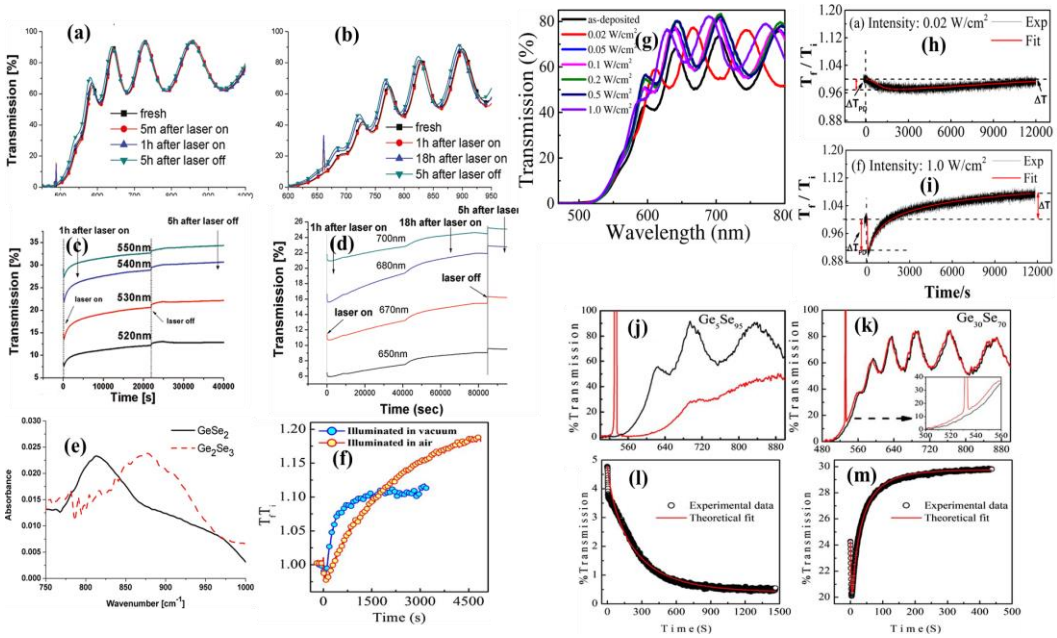

permission from [32] Copyright 2015, The Optical Society. (g) Transmission spectra of as-deposited $Ge_{16.8}Se_{83.2}$ film and the film irradiated by a laser with an power density of 0.02, 0.05, 0.1, 0.2, 0.5 and 1 W/cm², respectively. Time evolution of T_f/T_i of the films irradiated with a power density of (h) 0.02 and (i) 1 W/cm². All the figures were reprinted (adapted) with permission from [33] Copyright 2017, Springer Nature. Transmission spectra of (j) Ge_5Se_{95} and (k) $Ge_{30}Se_{70}$ before (solid black line) and after (solid red line) illumination with 532 nm laser light. Time evolution of T_f/T_i for the selected single-probe wavelength at 560 nm, when illuminated with the pump beam (532 nm) of intensity 0.5 W/cm² for (l) Ge_5Se_{95} and (m) $Ge_{30}Se_{70}$. Here the hollow circles and solid red line represent the experimental data and theoretical fit, respectively.

In another interesting work, Zhang *et al*. showed with proloned illumination can lead to PB even in Ge-deficient $Ge_{16.8}Se_{83.2}$ thin films [33]. Fig. 2(g) shows the transmission spectra of the sample when illuminated with 655 nm CW laser for a period of 12000 s at different intensities. Clearly, transmission spectra blueshifts to depict PB. To get more informationon, they perfored single wavelength kinetics at 560 nm at 0.02 and 1 W/cm² as shown in Fig. 2(h) and (i). At 0.02 W/cm², PD dominates with very weak and slow PB, whereas sample ends up in an overall PB state when illuminated with 1 W/cm². Therefore, excitation intensity plays a critical role in determining the overall behavior of the sample. Apart of that, kinetics of both PD and PB shows a strong dependence on laser power. For example, at 0.02 W/cm², reaction time of PD (τ_{PD} = 1200 s) and (τ_{PB} = 11000 s) is found to two orders slower when compared to 1 W/cm², where τ_{PD} = 36 s and τ_{PD} = 280 s, respectively. However, overall PD is instaneous woth laser ilumination always takes place faster than PB.

In similar line with more detailed work Kumar *et al*. showed that by varying the relative composition of Ge and Se, they obatain a crossover from PD to PB in Ge_xSe_{100-x} thin films

Preprints (www.preprints.org) | NOT PEER-REVIEWED | Posted: 2 March 2021 doi:10.20944/preprints202103.0057.v1

[34]. In this regard, Fig. 2(j) and (k) show the transmission spectra of Ge-deficent Ge_5Se_{95} and Ge-rich $Ge_{30}Se_{70}$ thin films in as-prepared (black) and illuminated (red) states when illuminated with 532 nm CW laser. The strong red shifted absorption edge depicts PD in the former, while weak blue shift in the later demonstrates PB. Singe wavelength kinetics at 560 nm for Ge_5Se_{95} and $Ge_{30}Se_{70}$ are shown in Fig. (l) and (m), respectively. For Ge_5Se_{95}, final transmission saturates much below the intial value in line with strong PD, whereas for $Ge_{30}Se_{70}$, the sample ends up in an overall PB state at the final stage of illumination.

2.3. Photobleaching and photobleaching in ternary Ge-As-Se

Termany Ge-As-Se forms a special family of ChGs which shows the unusual coexistence of fast PD and slow PB under CW illumination [18]. In addition, Ge-As-Se systems are advantageous since all the individual componenets have similar size and electronegativity and they form a close-to-ideal ChG network [35]. The structural connectivity in ChG is usually quantified by the mean coordination number Mean Coordination Number (MCN) as denoted by ⟨r⟩, where ⟨r⟩ is equal to the sum of the respective elemental concentrations times their covalent coordination number [36]. It is well known that physico-chemical properties of chalcogenides are strongly dependent on composition [19, 20] and that they appear to vary according to the mean coordination number ⟨r⟩ of the Phillips and Thorpe rigidity theory [37,38]. By calculating the angle constraints and bond length relative to the total number of degrees of freedom in an amorphous network by Philips [37] predicted the existence of a percolation transition at ⟨r⟩ = 2.40 from an under constrained "floppy" network to an over-constrained "rigid" one. In particular, many previous studies by Lucas and Calvez with cw illumination have shown that properties like PD, photorelaxation and photoexpansion exhibit an extremum at ⟨r⟩ = 2.4 with monotonic decreasing trend as shown in Fig. 3(a) and (b) [6,35,39]. In a stark contrast, by our previous work established that chemical composition plays major role and dominates over MCN in determining the lightinduced effects [40]. In this regard, Fig. 3(c) shows the single wavelength kinetics of a-$Ge_xAs_{35-x}Se_{65}$ (x=5, 10, 15 and 25) thin films. it is evident that upon pump beam illumination, T_f/T_i decreases instantaneously for all samples in a manner which is consistent with PD and eventually saturates within a few tens of seconds. After the complete saturation of PD, T_f/T_i for all samples except x=5 gradually starts increasing, a clear manifestation of PB. For the sample with x>15, PB saturates at a value which is above the as-prepared value and for the samples with x<15, PB saturates well below the as-prepared value. After the complete saturation of PD/PB, we also observed the transient compoent when the laser is switched off. In this context, for quantification PD and PB are calculated as the difference in transmission between initial (as prepared) and saturated value of PD and the difference between saturated values of PB and PD, respectively, as shown in Fig. 3(d). Fig. 3(e) shows that PD does not show a regular trend with MCN by vanishing at MCN=2.4, but decrease gradually with increasing MCN. On the other hand, in a stark contrast, in Fig. 3(f) PB linearly increases upto a MCN of 2.5 and then shows a sudden jump at 2.6. These results clearly demonstrate that PDand PB do not follow a regular trend as predicted by the network rigidity theory which is already discussed above, rather it is defined by the Ge:As composition ratio.

Preprints (www.preprints.org) | NOT PEER-REVIEWED | Posted: 2 March 2021 doi:10.20944/preprints202103.0057.v1

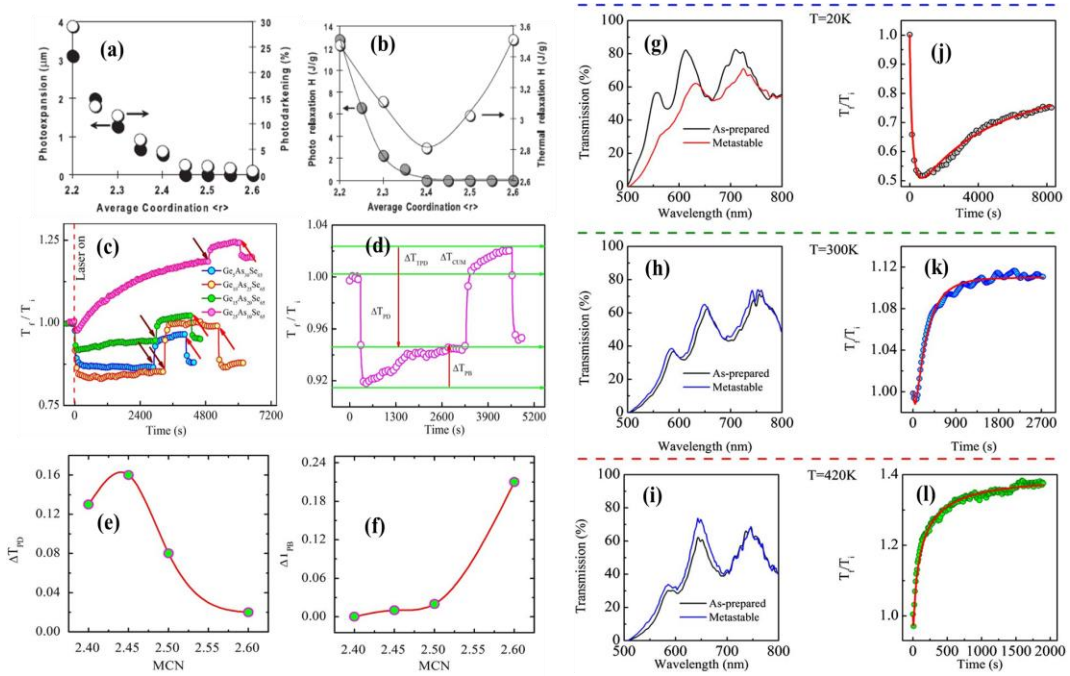

Figure 3. (a) Maximum photoexpansion and photodarkening as a function of network connectivity in a series of $Ge_xAs_xSe_{1-2x}$ glass irradiated with a tunable Ti:sapphire laser. (b) Comparison of photoinduced and thermally induced enthalpy relaxation in a series of $Ge_xAs_xSe_{1-2x}$ glass. Each sample was exposed to 3 W/cm^2 light until saturation or annealed at 25 ^{o}C below T_g for 80 h at which point no further relaxation was observed. All the figures were reprinted (adapted) with permission from [35] Copyright 2008, American Institute of Physics. (c) Temporal evolution of T_f/T_i of all a-$Ge_xAs_{35-x}Se_{65}$ thin films for the wavelength at which transmission is 20% of the value for the dark condition. Dashed line indicates the time at which laser was turned on. The downward (wine color) and upward (pink color) arrows represent the time at which laser is turned off and on respectively, showing the transient effects. (d) Schematic diagram showing the calculation of PD, TPD, PB and cumulative change in relative transmission for a-$Ge_{15}As_{20}Se_{65}$. Quantification of magnitude of (e) PD and (f) PB, as a function of MCNof the network. MCN increases from 2.4 to 2.6 when x increases from 5 to 25 in a- $Ge_xAs_{35-x}Se_{65}$ thin films. All the figures were reprinted (adapted) with permission from [40] Copyright 2014, Springer Nature. (g)-(i) represent the transmission spectra of a-$Ge_{25}As_{10}Se_{65}$ thin film in the as-prepared and post-illuminated states at 20, 300, and 420 K, respectively. (j)-(l) represent the temporal evolution of T_f/T_i for the wavelength at which the initial (dark) transmission is 10% at 20, 300, and 420 K, respectively.

In this context, there are some other interesting works by Yang *et al*. [19], Zhang *et al*. [41], Nemec *et al*. [42] who also demonstrated the CW laser illuminated lightinduced effects in Ge-As-Se thin films.

So far, we have seen that chemical composition, prolonged illumination, power density can be used as efficient tool to determing the lightindiced effects in ChGs. In our earlier work, we have showed that temperarure of illumination plays a very crucial role to control the lightinduced effects [7]. In this regard, Fig. 3(g)-(l) shows the temperature dependent lightinduced response in Ge rich $Ge_{25}As_{10}Se_{65}$ thin films at 20, 300 and 420 K. Rearkably, we found that by illuminaing at low temperature of 20 K, PD can be induced even in Ge rich $Ge_{25}As_{10}Se_{65}$ thin films as evinced by red shift and decrease in trasmission (top panel). At 300 K (middle panel), the sample exhibits expected weak PD follwed by strong PB. Light induced effects at 420K (bottom panel) show dramatically distinct characteristics when compared to 20 and 300 K. In this temperature, we could observe only negligible PD and PB start to dominate from the beginning. Further, the magnitude of PB is much higher than the room temperature values. Apart from that, reaction times for both PD and PB exhibits a strong dependence on illumintion temperature. Precisely, kinetics of both PD and PB become dramatically faster as temperature increases. We could

Preprints (www.preprints.org) | NOT PEER-REVIEWED | Posted: 2 March 2021 doi:10.20944/preprints202103.0057.v1

observe a significant decrease in both τ_{PD} (from 170 seconds to 3 seconds) and τ_{PB} (3600 seconds to 85 seconds) when illumination temperature is raised from 20 to 420 K. Such observations clearly indicate thermal vibration accelerates the kinetics of PD and PB at higher temperatures. Interesting to note that, when illuminated at high temperatures at 420 K, As_2Se_3/Ag/Se trilayer with no Ge content exhibits PB that tells us the importance of temperature in controlling lightinduced effects [43].

It is important to note that, apart from PD and PB, photo-diffusion and photo-dissolution is also quite common in bilayer film of metal and ChG when illuiminated with CW laser [44-49]. However, detailed discussion of such effects are beyond the scope of the present study. Nevertheless, such effects have tremendous potential application in lithography, hologram, photomasking etc.

3. Nanosecond (ns) lightinduced effects in ChGs

CW optical pump probe studies on PD/PB revealed that such effect consists of two parts: one is metastable PD/PB and the other is transient PD (TPD) which persists in the sample only during illumination [18,40]. Interestingly, it has been shown that for short illumination with a CW light, transient part is more apparent than the slow and cumulative metastable part. However, most of the previous studies on transient effects were performed with CW laser which has very low time resolution and consequently, an exact assessment of these effects remains rather unknown. In ChGs, time-of-flight (TOF) experiments emerged as a pioneer technique to study the lightinduced effects [50-52]. In TOF measurements, photocarriers created at one end of the sample drift across in an applied electric field, resulting in a current signal in the external circuit. First TOF measurements performed on As_2Se_3 with nitrogen-laser-pumped dye laser of wavelength 483 nm with a pulse duration of 10 ns [51] as shown in Fig. 4(a). In this experiment, holes are acted as carriers with a mobility that is characterized by a dispersive behavior over many orders of magnitude in time. TOF measurements at different temperatures in the range between 200 to 350 K show little deviation from the predicted power law behavior.

In another pioneer work, Tanaka aimed to understand the transient behavior of the photoinduced effects, which appear to be governed by lattice distortions [53]. In his work, Tanaka used As_2S_3 thin film and performed transient grating experiments with 488 nm, 5 ns pulsed laser to understand the time-resolved features of refractive index variation. Time evolution of lightinduced effects in annealed As_2S_3 sample with pulsed and biased CW laser is shown on top and middle panel of Fig. 4(b), respectively. For pulsed laser, the effect is irreversible as it does not decay to zero unlike CW, therefore can be exploited for optical memory devices. For the experiments performed at 80 K (bottom panel) with pulsed laser exhibits less effect with much slower time response since the band gap becomes wider with decreasing temperature and likewise absorption becomes smaller.

Similar to the work of Tanaka, Rosenblum and co-workers [54] tried to understand the dynamic as well as after-pulse effect in $As_{50}Se_{50}$ thin films by performing transient grating experiments using 532 nm, 5 ns, Nd:YAG laser. A dual time behavior is observed: the faster component, i.e., transient effect takes place in tens of nanosecond which is followed by asymptotically decayed slower component in the order of microseconds (Fig. 4(c)). Interestingly, the transient component scales a linear relationship with laser intensity, whereas the after pulsed effect varies quadratically with the laser intensity which indicates a nonlinear two-photon process associated with ChGs.

Preprints (www.preprints.org) | NOT PEER-REVIEWED | Posted: 2 March 2021 doi:10.20944/preprints202103.0057.v1

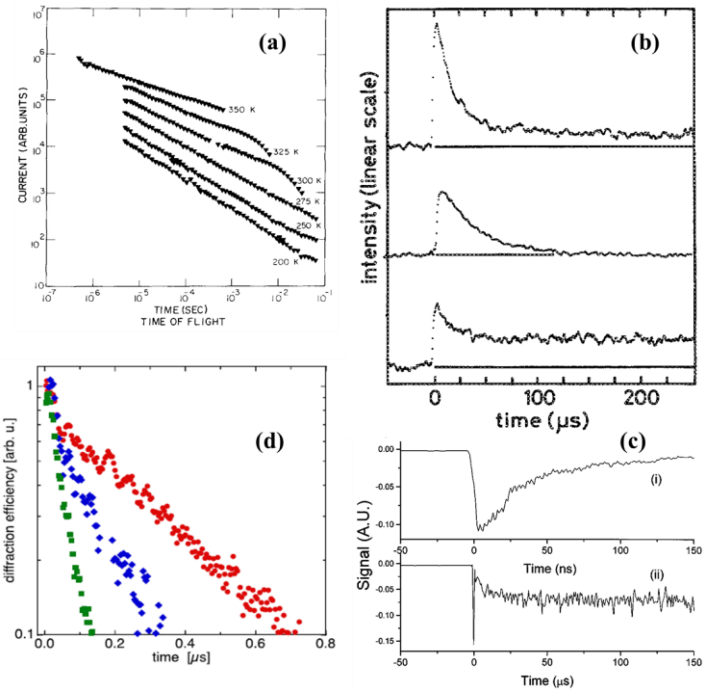

Figure 4. Time-of-flight current transients at various temperatures. The current decreases as a power law and the slope clearly decreases with increasing T. All the figures were reprinted (adapted) with permission from [51] Copyright 1983, Elsevier. (b) Typical responses of light intensities diffracted from grated As_2S_3, films in the annealed state (top), under bias illumination at room temperature (middle), and in annealed state at 80 K (bottom). The grating pitch is 25 μm. The profiles arc smoothed by a computer to increase signal-lo-noise ratio, and the time resolution is degrated to 2 μs. All the figures were reprinted (adapted) with permission from [53] Copyright 1989, American Institute of Physics. (c) Typical diffracted signal. A few tens of nanoseconds transient (i) is followed by a slow asymptotic response, the after-pulse effect (ii). The transient starts with the exciting pulse ~within our experimental error of ~ 1 ns. All the figures were reprinted (adapted) with permission from [54] Copyright 1999, American Institute of Physics. d)Time-dependence of the diffraction efficiency of a photoinduced transient grating in the a-As_2Se_3 film for three spatial periods of the illumination pattern. The shortest relaxation time is for a grating spacing of 0.7 μm. The two other data sets are for grating spacings of 1.1 μm and 1.6 μm, with the latter belonging to the longer relaxation time. All the figures were reprinted (adapted) with permission from [55] Copyright 2012, American Institute of Physics.

Much later in 2012, Regmi and colleagues performed pump-probe transient grating experiments in As_2Se_3 thin films with 532 nm laser, 20 ps laser [55]. The main difference between their work and earlier studies discussed above is that they pre-illuminated the sample with a bandgap laser until the sample completely become photodarkened permanently. Likewise, they cancel any permanent photoinduced change and focus only on nanosecond dynamics originating from short-lived excited states. In this regard, Fig. 4(d) depicts the time dependence of the diffraction efficiency that decays exponentially on the sub-microsecond time scale. The time constant consists of two part: excitonic lifetime and diffusion time and they are separated by changing transport length by varying the angle between the interfering beams. They experimentally demonstrated mobility that is 5 orders of magnitude larger than typical TOF mobilities [52].

Till now, in all these experiments, the transient effects are probed at a single wavelength and hence information on the induced absorption spectrum over a broad wavelength regime by ns excitation is not discussed. Similarly, the role of temperature and excitation fluence on the induced absorption and its kinetics are not established, although it is well apparent for CW illumination [18,40]. These issues were addressed by our previous work

Preprints (www.preprints.org) | NOT PEER-REVIEWED | Posted: 2 March 2021 doi:10.20944/preprints202103.0057.v1

in a-$Ge_xAs_{35-x}Se_{65}$ thin films, by performing ns transient absorption (TA) pump-probe measurements with 532 nm, 5 ns laser [16]. Fig. 5(a) demonstrates the change in absorbance (ΔA), i.e., TA of the samples at different MCN from 2.35 to 2.6 for the probe delay at 200 ns. We define $\Delta A=-\log(I_{es}/I_{gs})$, where, where I_{es} and I_{gs} are the transmitted intensities of probe pulses after delay time t following excitation by pump beam and in ground state respectively. We found that TA spectra is tunable, blue shift when x, in other words, the rigidity of the network increases.

Figure 5. (a) TA spectra of a-$Ge_xSs_{35-x}Se_{65}$ thin films at a probe delay of 200 ns. (b) Change in TA maxima with MCN. Evidently, TA decreases with increasing MCN. (c) Change in TA maximum for different MCN samples as a function of fluence. (d) Variation of decay time constant of TA for different MCN sample at different excitation fluence, which scales linearly. Colored symbols and the solid red line in each figure represent experimental data and theoretical fit, respectively. (e) Contour plot of time resolved transient absorption spectra of a-$Ge_5As_{30}Se_{65}$ thin film at 15 K, 165 K, 305 K and 405 K, when illuminated with 5 ns pulses of wavelength 532 nm. (f) Variation of decay time constant associated with TA_1 (τ_1) and TA_2 (τ_2) as a function of temperature. All the figures were reprinted (adapted) with permission from [56] Copyright 2014, Springer Nature. (g) Contour plot of the temporal and spectral evolution of the TA of ASP and BGI samples. The vertical dotted lines indicate the TA maxima. (h) Spectral evolution of the decay-time constant for ASP and BGI samples. Clearly, kinetics of TA is faster for BGI samples compared to ASP samples.

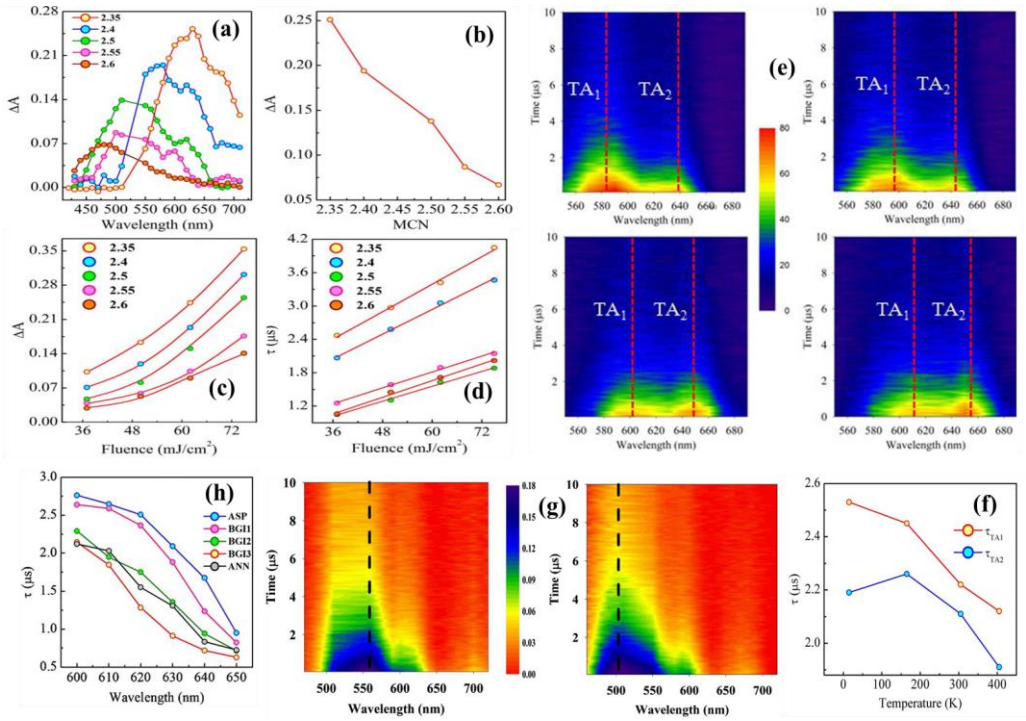

However, most importantly the magnitude of TA decreases dramatically with increasing MCN (Fig. 5(b)), by moving from floppy to rigid network as proposed by Phillips and Thorpe [37,38]. In fact, this observation provides the first direct experimental validation of network for ns pulsed illumination. We also validate the two-photon effect proposed by Rosenblum [54] by performing excitation fluence dependent TA study as shown in Fig. 5(c). As can be seen in the figure, TA maxima exhibits many folds increase with increasing fluence. Importantly, for all samples ΔA grows up non-linearly with excitation fluence and a second order polynomial equation fit very well to the experimental data. Such an observation suggests that the TA may be a two-photon process. This observation also fuels the idea of Lucas that irradiation with higher excitation fluence could induce adequate bond breaking or rearrangement to produce appreciable ΔA even in over-coordinated glasses (orange circles) as evident from the figure. Excitation fluence also affects the TA kinetics which is address by fitting single wavelength kinetics at TA maxima with one

Preprints (www.preprints.org) | NOT PEER-REVIEWED | Posted: 2 March 2021 doi:10.20944/preprints202103.0057.v1

decay constant (τ). Fig. 5(d) shows that τ exhibit a linear dependence with a negative slope on excitation fluence, i.e., TA is found to decay faster at lower fluence. The slow decay of TA at higher fluence can be understood by considering the fact that permanent structural changes become prominent which makes the relaxation process drastically slower.

We have already discussed the influence of temperature on CW lightinduced effects in terms of magnitude and kinetics of PD and PB [32,43]. Similar temperature dependence on ns lightinduced effect is also studied by our group in $Ge_5As_{30}Se_{65}$ thin films [56]. The 2-D contour plot of TA spectra at 15, 165, 300 and 405 K is shown in Fig. 5(e). Clearly, at all temperatures of illumination two discrete absorption bands TA_1 and TA_2 is observed. Existence of these transient dual absorption bands are in stark contrast to previous predictions of a broad featureless absorption based on small polaron model [57]. the rise of ΔA is instantaneous and decays within 10 μs, however the recovery was not complete within experimental time window. Notably, TA bands show a red shift with increase in temperature. This observation clearly demonstrates that the TA bands are thermally tunable, i.e., TA_1 shifts from 582 to 610 nm while TA_2 shifts from 638 to 657 nm when the temperature is raised from 15 to 405 K. Interestingly, TA_1 and TA_2 exhibit contrasting behavior with respect to temperature, i.e., while TA_1 decreases TA_2 increases with temperature. Precisely, at low and room temperatures TA_1 dominates over TA_2, however, at high temperature (405 K) TA_2 plays the predominant role. Nonetheless, the overall magnitude of TA by taking contributions from both TA_1 and TA_2, is found to be largest at low temperature. Temperature also has significant effect on the TA kinetics. From Fig. 5(f) both TA_1 (τ_1) and TA_2 (τ_2) decreases with increase in temperature, manifesting that the relaxation process becomes more rapid at higher temperatures, i.e., the relaxation of TA is a thermally activated process which indicates the transient defect states associated with it relaxes immediately at high temperature with the aid of thermal vibration. Similar temperature dependence is also obtained for As_2S_3 thin films for both 532 and 355 nm, 5ns laser excitation [58].

Controlling and tuning ns lightinduced effects is a very challenging problem which can be done very efficiently with a background illumination (BGI) since we already knew that CW light can significantly modify the structure of the ChGs to control the final state, whether darkened or bleached. In this regard, we have illuminated the $Ge_{25}As_{10}Se_{65}$ thin films continuously for nearly 2 hours with 532 nm CW laser until the sample gets completely photobleached. After we record the ns TA in as-prepared (ASP) and BGI samples as shown in Fig. 5(g) [59]. Strikingly, although the magnitude of TA remains the same, most importantly TA spectra of BGI sample dramatically blue shift from 560 nm to 500 nm compared to the ASP sample. We also found that blueshift increases linearly with the intensity of the CW illumination. In terms of kinetics, τ for the BGI samples are much smaller than for the ASP sample, i.e., the relaxation of TA is faster in the BGI samples (Fig. 5(h). Additionally, for both ASP and BGI samples, longer wavelength component of TA decay faster than the shorter wavelengths. Such observation clearly demonstrates that the photoexcited carriers have longer lifetime in the deep traps than in shallow traps [58].

4. Ultrafast lightinduced effects in ChGs

Femtosecond (fs) laser illuminated ultrafast lightinduced effects in ChG thin films are scarce until it was first demonstrated earlier by our group in $GeSe_2$ thin films [60]. The motivation is intrigued from the first principle molecular dynamic simulations [61] that shows light induced structural changes through defects occur at short (<500 fs) to long timescales (>500 fs) through the creating and annihilation of intimate valence alteration pairs (IVAPs) and VAPs, respectively [62,63]. To probe ultrafast lightinduced effects $GeSe_2$ thin films are excited with 100 fs, 400 nm and recorded the TA between 520– 740 nm probe wavelength as shown in the 2-D contour plot of Fig. 6(a) [60]. Several cross-sections of the contour at different probe delays are depicted in Fig. 6(b). Important features consist of 3 TA bands, long lived probe delays are shown in Fig. 6(b). T_1 and T_2 and a short lived T_3. T_1 and T_2 occurs at 650 and 610 nm respectively, from the VAPs. On the other hand, T_3

Preprints (www.preprints.org) | NOT PEER-REVIEWED | Posted: 2 March 2021 doi:10.20944/preprints202103.0057.v1

takes place between IVAPs at 725 nm. Since IVAPs are closed spaced they can self-annihilate easily, thus makes the kinetics faster. To get detailed analysis of the kinetics of ultrafast TA, global fitting by wavelength dependent decay associated spectra (DAS(λ)) is employed. In this regard, Fig. 6(c) depicts the temporal evolution of TA kinetics at selected probe wavelength of 610 and 730 nm, associated with VAP and IVAP, respectively. Two decay constants are obtained with DAS1 (fast) and DAS2 (slow) associated with τ_1= 4 ps and τ_2= 438 ps. As shown in Fig. 6(d) DAS1 dominates at longer wavelength, while DAS2 is dominant at shorter wavelength.

Figure 6. (a) Contour plot of TA spectra of $GeSe_2$ thin film in ps time. (b) TA at various probe delays at ps time. Time dependence of TA at 730 nm and 610 nm is shown in (c) time scales with corresponding theoretical fit. (d) Normalized DAS for different wavelengths in ps time scales. All the figures were reprinted (adapted) with permission from [60] Copyright 2014, Springer Nature. (e) TA spectra of a-Ge_xAs_{35}-xSe_{65} thin films for 400 nm excitation at probe delay of 1 ps. (f) Variation of TA amplitude for all samples in bandgap regions. Time evolution of central wavelength for (g) DAS1 and (h) DAS2. All the figures were reprinted (adapted) with permission from [64] Copyright

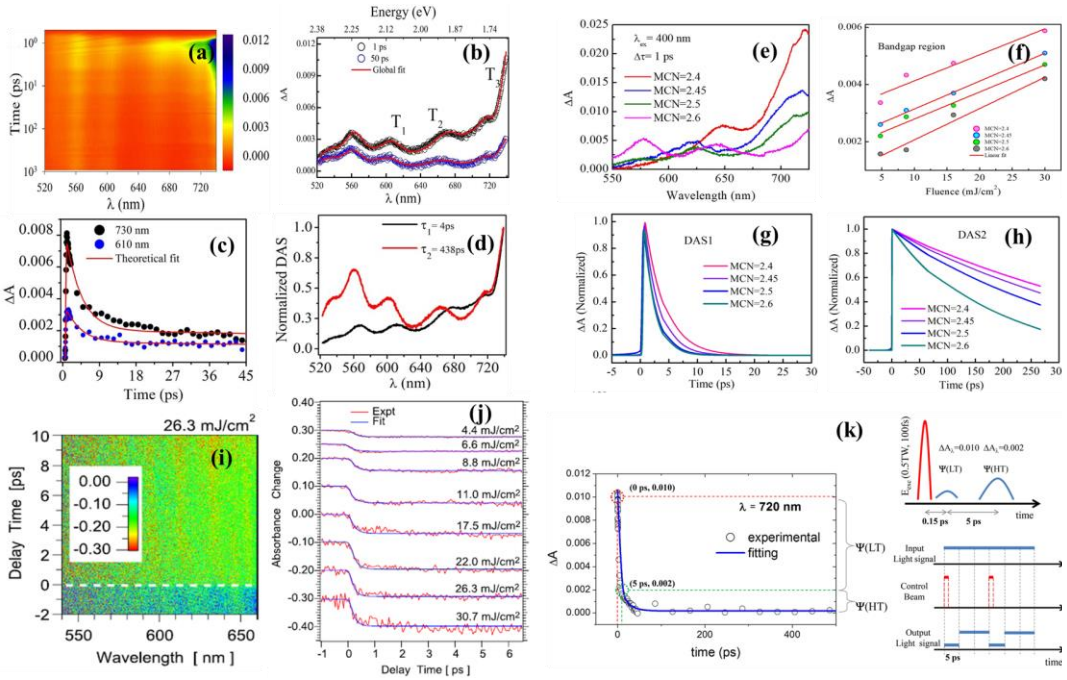

2018, American Institute of Physics. (i) 2D image of the TA change in crystalline GST film for a laser fluence of 26.3 mJ/cm². (j) Time evolution of the absorbance change in crystalline GST film for different laser fluences. All the figures were reprinted (adapted) with permission from [65] Copyright 2014, American Institute of Physics. (k) Ultrafast nonlinear response at 720 nm for AgNPs on semiconducting Se layer. Hollow circles and solid blue line represent experimental data and theoretical fit, respectively. DA drops to 20% of its maximum value within 5 ps after the pump beam excitation. We denote peak absorption as state of Low transmission state Ψ(LT) and 20% of peak absorption as state of High Transmission Ψ(HT) Schematic to show the effect of pump beam (red) onto probe beam (blue). Proposed application schematic of ultrafast response of AgNPs where output transmission can be modulated using a control beam. All the figures were reprinted (adapted) with permission from [66] Copyright 2013, American Institute of Physics.

We have seen earlier that ns TA in $Ge_xAs_{35-x}Se_{65}$ thin films decreases from floppy to rigid network in accordance with network rigidity theory [37,38]. To prove the validity of the theory under ultrafast pulsed excitation we performed femtosecond pump-probe measurements in $Ge_xAs_{35-x}Se_{65}$ thin films with 400 nm, 120 fs laser and the TA data for the samples are shown in Fig. 6(e) at probe delay of 1 ps [64]. Clearly, TA decreases when MCN increases from 2.4 to 2.6, however interestingly even beyond the rigidity percolation threshold the sample with MCN=2.6 shows significant TA which was not pedicted by network rigidity theory. In fact, with the increase in excitation flucne we could observe

Preprints (www.preprints.org) | NOT PEER-REVIEWED | Posted: 2 March 2021 doi:10.20944/preprints202103.0057.v1

manifold increase in the amplitude of TA for MCN=2.6 as well as for other samples in a linear fashion as shown in Fig. 6(f). Since Fig. 6(e) demonstrates that TA decay rates are different in different regions of the spectra, it calls for global DAS analysis over a broadband wavelength regime. In this regard, Fig. 6(g) and (h) show the kinetics of DAS1 and DAS2 (640 nm), from subdandgap (690-720 nm) and bandgap (600-640 nm) region, respectively. Clearly, DAS1 in the subbandgap region for all samples within 10s of picosecond (ps), that is associated with electron-lattice interaction. From Fig. 6(g) we found that the DAS1 curve is indisntinguishable for MCN 2.5 and 2.6, but least steep for MCN 2.4 that tells us electron-lattice interaction become slower in a lightly-constrained network compared to overconstrained ones. In stark contrast, DAS2 that is slower than DAS1 and occurs over few hundreds of ps, become steeper while transitioning from $\langle r \rangle$ = 2.40 to 2.60. Such observation indicates that exciton recombination and associated structural changes becomes faster over-constrained networks compared to lightly-constrained ones thanks to strong restoring forces of the rigid network. Numericall, τ_2 corresponding to DAS2 is found to be 417 ± 3, 355 ± 3, 271 ± 3, and 151 ± 2 ps for MCN 2.4, 2.45, 2.5 and 2.6 respectively.

Apart from Ge-As-Se, Ge-Sb-Se also requires special mention because of their application as a phase change material [67]. In this regard, Takeda *et al*. [65] studied the irreversible ultrafast crystalline-to-amorphous phase transition in $Ge_2Sb_2Te_5$ ChG alloy thin film with 100 fs, 800 nm laser by employing broadband single-shot imaging spectroscopy. In this regard, Fig. 6(i) depicts the 2-D contour plot of absorption with wavelength and time for a laser fluence 26.3 mJ/cm^2. Clearly, a rapid change is irreversible absorbance is observed that demonstrates the transition from crystalline to amorphous phase. A more consistent picture of phase change is depicted in Fig. 6(j) which shows the ultrafast temporal evolution of absorbane against the pump fluence. Absorption changes rapidly at all flucne within 1 ps. Below 6.6 mJ/cm^2, absorption recovers however, flucne higher than 8.8 mJ/cm2, absorption change is permanent this demonstrates the irreversible crystalline to amorphous phase change in GST material.

Ultrafast lightinduced effects have in a-Se/Ag bilayer ChG found tremendous potential application thanks to formation of spatially ordered and interconnected AgNPs on the surface of Se through optically driven diffusion [66]. The AgNP after the formation interact with intense femtosecond laser pulases and provide ultrafast optical response that can be exploited for application. In this regard, Fig. 6(k) shows the time evolution of kinetics curves of AgNP on Se at 720 nm. Clearly, the TA decays to 20 % of the maximum within a time period of 5 ps. By defining maximum absorbane as high transmission (HT) and 20 % absorbance as low trasmission (LT), the response can be utilized to make a optical switching device between HT to LT with a switching speed of 5 ps. As an example, a schematic of a optical modulator is shown in which the control pump beam modulates the transmission of signal probe beam. Ultrafast exciton-plasmon coupling has also been exploited to explore new functionalities in plasmon/ChG heterostructures which are unachievable by individual components [68].

5. Conclusions

This In this review, we covered two contrasting important aspects of lightinduced effects in ChGs separated by the pulse-duration of the excitation laser. In the first part, we demonstrated that PD and PB takes place under CW illumination through homopolar to heteropolar bond conversion and are predominantly metastable with negligible transient component. We showed that by tuning the chemical composition of the individual components, PD and PB can be tuned. Moreover, we found that PD is dominant at lower and room temperature while PB dominates at high temperature through photo-oxidation. In the second part, we demonstrated that under pulsed laser illumination, TA takes place via exciton self-trapping. Importantly, unlike CW illumination, for pulsed laser, lightinduced

effects decrease from floppy to rigid network in accordance with network rigidity theory. Apart from that, several studies show that TA can be spectrally tunable with temperature of illumination as well as via background CW illumination.

Author Contributions: P.K. wrote and edited the draft. P.K. and K.V.A have agreed to the published version of the manuscript.

Funding: This research was funded by Science and Engineering Research Board (Project No. EMR/2016/002520), Council of Scientific and Industrial Research, India (Grant No. 03 (1250)/12/EMR-II), and DAE BRNS (Sanction No. 37(3)/ 14/26/2016-BRNS/37245).

Conflicts of Interest: The authors declare no conflict of interest.

References

1. Shimakawa, K.; Kolobov, A.; Elliott, S.R. Photoinduced effects and metastability in amorphous semiconductors and insulators. *Advances in Physics* **1995**, *44*, 475-588, doi:10.1080/00018739500101576.
2. Sharma, P.; Sharma, N.; Sharda, S.; Katyal, S.C.; Sharma, V. Recent developments on the optical properties of thin films of chalcogenide glasses. *Progress in Solid State Chemistry* **2016**, *44*, 131-141, doi:https://doi.org/10.1016/j.progsolidstchem.2016.11.002.
3. Bureau, B.; Zhang, X.H.; Smektala, F.; Adam, J.-L.; Troles, J.; Ma, H.-l.; Boussard-Plèdel, C.; Lucas, J.; Lucas, P.; Le Coq, D., et al. Recent advances in chalcogenide glasses. *Journal of Non-Crystalline Solids* **2004**, *345-346*, 276-283, doi:https://doi.org/10.1016/j.jnoncrysol.2004.08.096.
4. Watts, R.K.; de Wit, M.; Holton, W.C. Nonoxide chalcogenide glass films for integrated optics. *Appl Opt* **1974**, *13*, 2329-2332, doi:10.1364/AO.13.002329.
5. Bruno, B.; Catherine, B.; Shuo, C.; Radwan, C.; Marie-Laure, A.; Virginie, N.; Olivier, S.; Olivier, L.; Pierre, L.; Valerie, M., et al. Chalcogenide optical fibers for mid-infrared sensing. *Optical Engineering* **2014**, *53*, 1-8, doi:10.1117/1.OE.53.2.027101.
6. Calvez, L.; Yang, Z.; Lucas, P. Composition dependence and reversibility of photoinduced refractive index changes in chalcogenide glass. *Journal of Physics D: Applied Physics* **2010**, *43*, 445401, doi:10.1088/0022-3727/43/44/445401.
7. Khan, P.; Bhattacharya, A.; Joshy, A.; Sathe, V.; Deshpande, U.; Adarsh, K.V. Investigation of temperature dependent optical modes in GexAs35−xSe65 thin films: Structure specific Raman, FIR and optical absorption spectroscopy. *Thin Solid Films* **2017**, *621*, 76-83, doi:https://doi.org/10.1016/j.tsf.2016.11.037.
8. Eggleton, B.J.; Luther-Davies, B.; Richardson, K. Chalcogenide photonics. *Nature Photonics* **2011**, *5*, 141-148, doi:10.1038/nphoton.2011.309.
9. Street, R.A. Non-radiative recombination in chalcogenide glasses. *Solid State Communications* **1977**, *24*, 363-365, doi:https://doi.org/10.1016/0038-1098(77)90983-8.
10. Street, R.A. Recombination in a-Si: H: Spin-dependent effects. *Physical Review B* **1982**, *26*, 3588-3604, doi:10.1103/PhysRevB.26.3588.
11. Halpern, V. On the photoconductivity of amorphous chalcogenide semiconductors. *Philosophical Magazine B* **1978**, *37*, 423-434, doi:10.1080/01418637808225787.
12. Kastner, M.; Adler, D.; Fritzsche, H. Valence-Alternation Model for Localized Gap States in Lone-Pair Semiconductors. *Physical Review Letters* **1976**, *37*, 1504-1507, doi:10.1103/PhysRevLett.37.1504.
13. Ganjoo, A.; Jain, H. Millisecond kinetics of photoinduced changes in the optical parameters of $\mathrm{a}\text{\ensuremath{-}}{\mathrm{As}}_{2}{\mathrm{S}}_{3}$ films. *Physical Review B* **2006**, *74*, 024201, doi:10.1103/PhysRevB.74.024201.
14. Ganjoo, A.; Shimakawa, K.; Kitano, K.; Davis, E.A. Transient photodarkening in amorphous chalcogenides. *Journal of Non-Crystalline Solids* **2002**, *299-302*, 917-923, doi:https://doi.org/10.1016/S0022-3093(01)00991-7.

15. Barik, A.R.; Bapna, M.; Drabold, D.A.; Adarsh, K.V. Ultrafast light induced unusually broad transient absorption in the sub-bandgap region of GeSe2 thin film. *Sci Rep* **2014**, *4*, 3686, doi:10.1038/srep03686.
16. Khan, P.; Saxena, T.; Adarsh, K.V. Tailoring between network rigidity and nanosecond transient absorption in a-Ge(x)As(35-x)Se(6)(5) thin films. *Opt Lett* **2015**, *40*, 768-771, doi:10.1364/OL.40.000768.
17. Berkes, J.S.; Ing, S.W.; Hillegas, W.J. Photodecomposition of Amorphous As2Se3 and As2S3. *Journal of Applied Physics* **1971**, *42*, 4908-4916, doi:10.1063/1.1659873.
18. Khan, P.; Barik, A.R.; Vinod, E.M.; Sangunni, K.S.; Jain, H.; Adarsh, K.V. Coexistence of fast photodarkening and slow photobleaching in Ge19As21Se60 thin films. *Opt Express* **2012**, *20*, 12416-12421, doi:10.1364/OE.20.012416.
19. Yang, G.; Jain, H.; Ganjoo, A.; Zhao, D.; Xu, Y.; Zeng, H.; Chen, G. A photo-stable chalcogenide glass. *Opt Express* **2008**, *16*, 10565-10571, doi:10.1364/oe.16.010565.
20. Antoine, K.; Jain, H.; Vlcek, M.; Senanayake, S.D.; Drabold, D.A. Chemical origin of polarization-dependent photoinduced changes in an ${\text{As}}_{36}{\text{Se}}_{64}$ glass film via in situ synchrotron x-ray photoelectron spectroscopy. *Physical Review B* **2009**, *79*, 054204, doi:10.1103/PhysRevB.79.054204.
21. Lyubin, V.; Klebanov, M.; Bruner, A.; Shitrit, N.; Sfez, B. Transient photodarkening and photobleaching in glassy GeSe2 films. *Optical Materials* **2011**, *33*, 949-952, doi:https://doi.org/10.1016/j.optmat.2010.11.028.
22. Yan, Q.; Jain, H.; Ren, J.; Zhao, D.; Chen, G. Effect of Photo-Oxidation on Photobleaching of GeSe2 and Ge2Se3 Films. *The Journal of Physical Chemistry C* **2011**, *115*, 21390-21395, doi:10.1021/jp2035967.
23. Spence, C.A.; Elliott, S.R. Light-induced oxidation and band-edge shifts in thermally evaporated films of germanium chalcogenide glasses. *Physical Review B* **1989**, *39*, 5452-5463, doi:10.1103/PhysRevB.39.5452.
24. Tichý, L.; Tichá, H.; Nagels, P.; Sleeckx, E. A review of the specific role of oxygen in irreversible photo- and thermally induced changes of the optical properties of thin film amorphous chalcogenides. *Optical Materials* **1995**, *4*, 771-779, doi:https://doi.org/10.1016/0925-3467(95)00022-4.
25. Mori, T.; Hosokawa, N.; Shimakawa, K. Dynamics of photodarkening in amorphous As2Se3 films: In situ simultaneous measurements of optical transmittance and photocurrent. *Journal of Non-Crystalline Solids* **2008**, *354*, 2683-2686, doi:https://doi.org/10.1016/j.jnoncrysol.2007.09.089.
26. Sati, D.C.; Kumar, R.; Mehra, R.M.; Jain, H.; Ganjoo, A. Kinetics of photodarkening in a-As2Se3 thin films. *Journal of Applied Physics* **2009**, *105*, 123105, doi:10.1063/1.3151804.
27. van Popta, A.; Decorby, R.; Haugen, C.; Robinson, T.; McMullin, J.; Tonchev, D.; Kasap, S. Photoinduced refractive index change in As2Se3 by 633nm illumination. *Opt Express* **2002**, *10*, 639-644, doi:10.1364/oe.10.000639.
28. Swanepoel, R. Determination of the thickness and optical constants of amorphous silicon. *Journal of Physics E: Scientific Instruments* **1983**, *16*, 1214-1222, doi:10.1088/0022-3735/16/12/023.
29. de L. Kronig, R. On the Theory of Dispersion of X-Rays. *J. Opt. Soc. Am.* **1926**, *12*, 547-557, doi:10.1364/JOSA.12.000547.
30. Barik, A.R.; Naik, R.; Adarsh, K.V. Unusual observation of fast photodarkening and slow photobleaching in a-GeSe2 thin film. *Journal of Non-Crystalline Solids* **2013**, *377*, 179-181, doi:https://doi.org/10.1016/j.jnoncrysol.2013.01.038.
31. Liu, Y.; Jain, H.; Ren, J.; Yan, Q.; Chen, G. High-Resolution X-ray Photoelectron Spectroscopy Study of Photo-Oxidation of Amorphous Oxy-Chalcogenide Films. *The Journal of Physical Chemistry C* **2012**, *116*, 24590-24595, doi:10.1021/jp3072712.
32. Khan, P.; Sharma, R.; Deshpande, U.; Adarsh, K.V. First observation of the temperature-dependent light-induced response of Ge(25)As(10)Se(65) thin films. *Opt Lett* **2015**, *40*, 1559-1562, doi:10.1364/OL.40.001559.
33. Zhang, S.; Chen, Y.; Wang, R.; Shen, X.; Dai, S. Observation of photobleaching in Ge-deficient Ge 16.8 Se 83.2 chalcogenide thin film with prolonged irradiation. *Scientific Reports* **2017**, *7*, 14585, doi:10.1038/s41598-017-14796-w.
34. Kumar, R.R.; Barik, A.R.; Vinod, E.M.; Bapna, M.; Sangunni, K.S.; Adarsh, K.V. Crossover from photodarkening to photobleaching in a-Ge(x)Se(100-x) thin films. *Opt Lett* **2013**, *38*, 1682-1684, doi:10.1364/OL.38.001682.
35. Calvez, L.; Yang, Z.; Lucas, P. Light-Induced Matrix Softening of Ge-As-Se Network Glasses. *Physical Review Letters* **2008**, *101*, 177402, doi:10.1103/PhysRevLett.101.177402.

36. Wang, R.P.; Bulla, D.; Smith, A.; Wang, T.; Luther-Davies, B. Structure and physical properties of GexAsySe1−x−y glasses with the same mean coordination number of 2.5. *Journal of Applied Physics* **2011**, *109*, 023517, doi:10.1063/1.3544309.
37. Phillips, J.C. Topology of covalent non-crystalline solids I: Short-range order in chalcogenide alloys. *Journal of Non-Crystalline Solids* **1979**, *34*, 153-181, doi:https://doi.org/10.1016/0022-3093(79)90033-4.
38. Thorpe, M.F. Continuous deformations in random networks. *Journal of Non-Crystalline Solids* **1983**, *57*, 355-370, doi:https://doi.org/10.1016/0022-3093(83)90424-6.
39. Lucas, P. Energy landscape and photoinduced structural changes in chalcogenide glasses. *Journal of Physics: Condensed Matter* **2006**, *18*, 5629-5638, doi:10.1088/0953-8984/18/24/005.
40. Khan, P.; Jain, H.; Adarsh, K.V. Role of Ge:As ratio in controlling the light-induced response of a-Ge x As 35−x Se 65 thin films. *Scientific Reports* **2014**, *4*, 4029, doi:10.1038/srep04029.
41. Zhang, Z.; Xu, S.; Chen, Y.; Shen, X.; Wang, R. Photo-induced effects in Ge-As-Se films in various states. *Opt. Mater. Express* **2020**, *10*, 540-548, doi:10.1364/OME.385115.
42. Němec, P.; Zhang, S.; Nazabal, V.; Fedus, K.; Boudebs, G.; Moreac, A.; Cathelinaud, M.; Zhang, X.H. Photo-stability of pulsed laser deposited GexAsySe100-x-y amorphous thin films. *Opt. Express* **2010**, *18*, 22944-22957, doi:10.1364/OE.18.022944.
43. Khan, P.; Joshy, A.; Bhattacharya, A.; Adarsh, K.V. Observation of giant photodarkening and temperature mediated transition to photobleaching in As2Se3/Ag/Se trilayer. *Journal of Non-Crystalline Solids* **2016**, *449*, 70-74, doi:https://doi.org/10.1016/j.jnoncrysol.2016.07.022.
44. Mitkova, M.; Kozicki, M.N. Ag-photodoping in Ge-chalcogenide amorphous thin films—Reaction products and their characterization. *Journal of Physics and Chemistry of Solids* **2007**, *68*, 866-872, doi:https://doi.org/10.1016/j.jpcs.2007.01.004.
45. Wagner, T.; Ewen, P.J.S. Photo-induced dissolution effect in Ag/As33S67 multilayer structures and its potential application. *Journal of Non-Crystalline Solids* **2000**, *266-269*, 979-984, doi:https://doi.org/10.1016/S0022-3093(99)00890-X.
46. Khan, P.; Xu, Y.; Leon, W.; Adarsh, K.V.; Vezenov, D.; Biaggio, I.; Jain, H. Kinetics of photo-dissolution within Ag/As2S3 heterostructure. *Journal of Non-Crystalline Solids* **2018**, *500*, 468-474, doi:https://doi.org/10.1016/j.jnoncrysol.2018.09.001.
47. Palumbo, V.P.; Kovalskiy, A.; Jain, H.; Huey, B.D. Direct investigation of silver photodissolution dynamics and reversibility in arsenic trisulphide thin films by atomic force microscopy. *Nanotechnology* **2013**, *24*, 125706, doi:10.1088/0957-4484/24/12/125706.
48. Binu, S.; Khan, P.; Barik, A.R.; Sharma, R.; Golovchak, R.; Jain, H.; Adarsh, K.V. Photoinduced formation of Ag nanoparticles on the surface of As2S3/Ag thin bilayer. *Materials Research Express* **2014**, *1*, 045025, doi:10.1088/2053-1591/1/4/045025.
49. Kolobov, A.V.; Elliott, S.R. Photodoping of amorphous chalcogenides by metals. *Advances in Physics* **1991**, *40*, 625-684, doi:10.1080/00018739100101532.
50. Pfister, G.; Scher, H. Dispersive (non-Gaussian) transient transport in disordered solids. *Advances in Physics* **1978**, *27*, 747-798, doi:10.1080/00018737800101474.
51. Khan, B.A.; Kastner, M.A.; Adler, D. Time-of-flight and photoconductivity studies of a-As2Se3 films. *Solid State Communications* **1983**, *45*, 187-189, doi:https://doi.org/10.1016/0038-1098(83)90373-3.
52. Owen, A.E.; Robertson, J.M. Electronic properties of some simple chalcogenide glasses. *Journal of Non-Crystalline Solids* **1970**, *2*, 40-51, doi:https://doi.org/10.1016/0022-3093(70)90119-5.
53. Tanaka, K. Transient-grating study of amorphous As2S3 films. *Journal of Applied Physics* **1989**, *65*, 2042-2046, doi:10.1063/1.342872.
54. Rosenblum, G.; Sfez, B.G.; Kotler, Z.; Lyubin, V.; Klebanov, M. Nonlinear optical effects in chalcogenide photoresists. *Applied Physics Letters* **1999**, *75*, 3249-3251, doi:10.1063/1.125314.
55. Regmi, A.; Ganjoo, A.; Zhao, D.; Jain, H.; Biaggio, I. Fast excited state diffusion in a-As2Se3 chalcogenide films. *Applied Physics Letters* **2012**, *101*, 061911, doi:10.1063/1.4745612.
56. Khan, P.; Saxena, T.; Jain, H.; Adarsh, K.V. Nanosecond light induced, thermally tunable transient dual absorption bands in a-Ge 5 As 30 Se 65 thin film. *Scientific Reports* **2014**, *4*, 6573, doi:10.1038/srep06573.

57. Emin, D. Dynamics of the optically induced properties of a small-polaronic glass. *Journal of Non-Crystalline Solids* **1980**, *35-36*, 969-973, doi:https://doi.org/10.1016/0022-3093(80)90326-9.
58. Khan, P.; Acharja, P.; Joshy, A.; Bhattacharya, A.; Kumar, D.; Adarsh, K.V. Nanosecond light-induced transient absorption in As2S3: Self-trapped exciton recombination in amorphous chalcogenides. *Journal of Non-Crystalline Solids* **2015**, *426*, 72-77, doi:https://doi.org/10.1016/j.jnoncrysol.2015.07.002.
59. Khan, P.; Yadav, R.K.; Bhattacharya, A.; Joshy, A.; Aneesh, J.; Adarsh, K.V. Tuning nanosecond transient absorption in a-Ge(2)(5)As(1)(0)Se(6)(5) thin films via background illumination. *Opt Lett* **2015**, *40*, 4512-4515, doi:10.1364/OL.40.004512.
60. Barik, A.R.; Bapna, M.; Drabold, D.A.; Adarsh, K.V. Ultrafast light induced unusually broad transient absorption in the sub-bandgap region of GeSe 2 thin film. *Scientific Reports* **2014**, *4*, 3686, doi:10.1038/srep03686.
61. Li, J.; Drabold, D.A. Direct Calculation of Light-Induced Structural Change and Diffusive Motion in Glassy ${\mathrm{As}}_{2}{\mathrm{Se}}_{3}$. *Physical Review Letters* **2000**, *85*, 2785-2788, doi:10.1103/PhysRevLett.85.2785.
62. Zhang, X.; Drabold, D.A. Direct Molecular Dynamic Simulation of Light-Induced Structural Change in Amorphous Selenium. *Physical Review Letters* **1999**, *83*, 5042-5045, doi:10.1103/PhysRevLett.83.5042.
63. Zhang, X.; Drabold, D.A. SIMULATION OF THE RESPONSE OF AMORPHOUS SELENIUM TO LIGHT. *International Journal of Modern Physics B* **2001**, *15*, 3190-3196, doi:10.1142/S0217979201007476.
64. Khan, P.; Yadav, R.K.; Adarsh, K.V. Ultrafast light-induced softening of chalcogenide thin films above the rigidity percolation transition. *Journal of Applied Physics* **2018**, *124*, 125702, doi:10.1063/1.5050555.
65. Takeda, J.; Oba, W.; Minami, Y.; Saiki, T.; Katayama, I. Ultrafast crystalline-to-amorphous phase transition in Ge2Sb2Te5 chalcogenide alloy thin film using single-shot imaging spectroscopy. *Applied Physics Letters* **2014**, *104*, 261903, doi:10.1063/1.4886969.
66. Bapna, M.; Sharma, R.; Barik, A.R.; Khan, P.; Ranjan Kumar, R.; Adarsh, K.V. Light induced diffusion driven self assembly of Ag nanoparticles in a-Se/Ag bi-layer thin film with ultrafast optical response. *Applied Physics Letters* **2013**, *102*, 213110, doi:10.1063/1.4807934.
67. Guo, P.; Sarangan, A.M.; Agha, I. A Review of Germanium-Antimony-Telluride Phase Change Materials for Non-Volatile Memories and Optical Modulators. *Applied Sciences* **2019**, *9*, doi:10.3390/app9030530.
68. Sharma, R.; Khan, P.; Aneesh, J.; Sangunni, K.S.; Csarnovics, I.; Kokenyesi, S.; Jain, H.; Adarsh, K.V. Strong exciton-localized plasmon coupling in a-Ge24Se76/AuNP heterostructure. *APL Materials* **2016**, *4*, 106105, doi:10.1063/1.4964365.